DESY–21–xxx
Draft version 1.0
18th March 2021

Azimuthal correlations in photoproduction and deep inelastic *ep* scattering at HERA and indications of multiparton interactions

ZEUS Collaboration

Abstract

Collective behaviour and multiparton interactions are studied in high-multiplicity *ep* scattering at a centre-of-mass energy $\sqrt{s} = 318$ GeV with the ZEUS detector at HERA. Two- and four-particle azimuthal correlations as well as multiplicity, transverse momentum, and pseudorapidity distributions for event multiplicities $N_{\rm ch} \geq 20$ are measured. The dependence of two-particle correlations on the virtuality of the exchanged photon clearly distinguish photoproduction from neutral current deep inelastic scattering. The measurements in photoproduction processes and neutral current deep inelastic scattering do not indicate significant collective behaviour like those observed in high-multiplicity hadronic collisions at RHIC and the LHC. Comparisons of PYTHIA predictions with the measurements in photoproduction strongly indicate the presence of multiparton interactions from hadronic fluctuations of the exchanged photon.

1 Introduction

A wide variety of measurements in heavy-ion collisions indicate the formation of a new state of quark-gluon matter in a local thermal equilibrium [1–6]. One of the key observables of the quark–gluon plasma (QGP) is the collective behaviour of final-state particles. Recent striking measurements from smaller colliding systems such as $p+p$, $p+A$, and photo-nuclear $A+A$ suggest that a QGP may even form in systems previously thought too small to attain thermal equilibrium [7–14]. The first search for collective behavior in neutral current deep inelastic ep scattering was performed by the ZEUS experiment at the Hadron Electron Ring Accelerator (HERA) by studying two-particle azimuthal correlations, which did not strongly resemble those observed at RHIC and the LHC [15].

Two regimes of ep scattering are distinguished by the virtuality of the exchanged photon between the electron and proton, which is defined using the four-momentum difference between the incoming and scattered electron as: $Q^2 \equiv -q^2 = -(k - k')^2$. Neutral Current Deep Inelastic Scattering (NC DIS) occurs at large virtuality of the exchange photon ($Q^2 \gg \Lambda^2_{\mathrm{QCD}} \approx (200\ \mathrm{MeV})^2$), which strikes a single quark within the proton. Photoproduction (PhP) processes are defined for quasi-real exchange photons ($Q^2 \lesssim \Lambda^2_{\mathrm{QCD}}$), and is further sub-divided into two categories at leading order: direct and resolved. In direct photoproduction, the photon couples directly to a quark as in DIS. Resolved photoproduction, on the other hand, occurs when the photon fluctuates into partons, which then scatters with one or more partons in the proton. The resolved photoproduction and DIS regimes are illustrated in Fig. 1.

The possibility of observing multiple distinct $2 \to 2$ initial partonic scatterings in a single ep collision can be investigated with photoproduction at HERA. Such Multiparton Interactions (MPI) become a possibility for resolved photoproduction. While they are an essential ingredient in high-multiplicity hadronic collisions at the LHC, they have not been observed conclusively so far in lepton-hadron collisions.

Heavy-ion collisions present a scenario that is characterized by an extreme degree of MPI. A fully overlapping collision between two lead nuclei, with over 200 nucleons each, may lead to as much as 1000 binary nucleon collisions [16]. Each individual binary collision may additionally induce multiple partonic scatterings, allowing for several thousands of MPI in a single event. Many measurements in heavy-ion collisions indicate that this dense and extended initial state lays the foundation for a prominent stage of rescattering between partons, which rapidly forms a local thermal equilibrium. The resulting fluid of QCD matter (the QGP) can be described within the framework of relativistic hydrodynamcs [17–19].

Photoproduction at HERA provides the opportunity to study MPI and a potential rescattering stage in substantially smaller initial states. The space-time extent that is probed by the photon in a scattering process can be characterized by its de Broglie wavelength and the coherence length of its hadronic fluctuations [20]. The exchanged photon with four-momentum q, possesses a temporal, transverse, and longitudinal wavelength given by $1/q_0$, $1/q_T$, and $1/q_L$, respectively. The general resolving power increases with the virtuality of the photon and is given by $1/|Q|$. Both the coherence length and the wavelengths tend to zero for sufficiently large Q^2 and Bjorken x and in such cases the photon acts as a point-like probe of the proton. Thus, the probed region in DIS is typically much smaller than the proton while in photoproduction it can be the full size of the proton itself and may therefore resemble the spatial extents produced in $p + p$ and $p + A$ collisions.

A view of the collision zone in the plane transverse to the beam axis in resolved photoproduction is shown in Fig. 2. The spatial distribution of the zone is in general irregular but one with a dominant elliptical eccentricity[1] is shown. Frequently in heavy-ion collisions, such an elliptical component is caused persistently by the geometrical nature of spherical nuclei which do not fully overlap during the collision. However, in ep, $p + p$, and $p + A$, elliptical components arise purely from event-by-event fluctuations of parton distributions. Three spatially separated MPI centres are depicted as sources of gluons which may further rescatter with other gluons in the system. Intra- and cross-MPI rescattering are shown whereby gluons interact within or across separate MPIs, respectively. Numerous cross-MPI rescatterings are expected to be essential to the collective particle production in heavy-ion collisions. The possibility of a spatially-extended MPI zone and a subsequent rescattering stage in ep photoproduction thus provides an important step of understanding along the path from fundamental DIS to larger hadronic systems, where collective behaviour has been observed.

Azimuthal correlations are sensitive to the dynamics of the collision zone. Depending on the degree of rescattering, the eccentricities of the deposited matter in the initial state can be converted into a momentum asymmetry of the produced particles [22–25]. The eccentricity depicted in Fig. 2 would lead to an elliptical asymmetry in final-state particle momenta. Two-particle azimuthal correlations can be used to quantify the asymmetries but may be biased by unrelated two-body correlations such as resonance decays. Four-particle cumulant correlations are more robust to such biases as they are explicitly subtracted off in their construction.

In this article, measurements sensitive to collective fluid-like behaviour and MPI in ep scattering at high multiplicity $N_{\mathrm{ch}} \geq 20$ are presented. These measurements complement a previous ZEUS study of azimuthal correlations in NC DIS [15]. In photoproduction,

[1] Eccentricities are commonly used to characterise the profile of the initial state in heavy-ion collisions [21].

measurements are made of the charged particle multiplicity, pseudorapidity, and transverse momentum distributions as well as two- and four-particle azimuthal correlations. Two-particle azimuthal correlations are shown as a function of Q^2 to illustrate their evolution from photoproduction to DIS. The possibility of MPI in photoproduction is investigated by comparing the measured distributions and correlation functions to predictions from the PYTHIA event generator [26].

2 Experimental set-up and data selection

The photoproduction and NC DIS data used in this analysis were taken with the ZEUS detector at HERA during 2003-2007 (HERA II). During this period, the HERA accelerator collided 27.5 GeV electron/positron[2] beams with 920 GeV proton beams, which yields a nominal centre-of-mass energy of $\sqrt{s} = 318\,\text{GeV}$. This analysis uses an integrated luminosity of $366 \pm 7\,\text{pb}^{-1}$ recorded by ZEUS in HERA II at this energy.

A detailed description of the ZEUS detector[3] can be found elsewhere [27]. In the kinematic range of the analysis, charged particles were mainly tracked in the central tracking detector (CTD) [28–30] and the microvertex detector (MVD) [31]. These components operated in a magnetic field of 1.43 T provided by a thin superconducting solenoid. The high-resolution uranium–scintillator calorimeter (CAL) [32–35] consisted of three parts: the forward (FCAL), the barrel (BCAL) and the rear (RCAL) calorimeters. Each part was subdivided transversely into towers and longitudinally into one electromagnetic section (EMC) and either one (in RCAL) or two (in BCAL and FCAL) hadronic sections (HAC).

The ZEUS experiment operated a three-level trigger system [36,37]. For the NC DIS part of this analysis, events were selected at the first level if they had an energy deposit in the CAL consistent with an isolated scattered electron. At the second level, a requirement on the energy and longitudinal momentum of the event was used to select NC DIS event candidates. At the third level, the full event was reconstructed and tighter requirements for a DIS electron were made. For the photoproduction analysis, an inclusive set of triggers does not exist. Instead, triggers designed to capture heavy-flavour decays and jets were

[2] Hereafter, "electron" refers to both electrons and positrons unless otherwise stated. HERA operated with electron beams during 2005 and part of 2006, while positrons were accelerated in the other years of this data sample.

[3] The ZEUS coordinate system is a right-handed Cartesian system, with the Z axis pointing in the nominal proton beam direction, referred to as the "forward direction", and the X axis pointing left towards the centre of HERA. The coordinate origin is at the centre of the CTD. The pseudorapidity is defined as $\eta = -\ln\left(\tan\frac{\theta}{2}\right)$, where the polar angle, θ, is measured with respect to the Z axis. The azimuthal angle, φ, is measured with respect to the X axis.

utilized and their corresponding biases to an inclusive measurement were estimated and corrected for using Monte Carlo data with the ZEUS detector simulation. Only high-multiplicity events were retained in order to minimize the bias to this analysis.

Photoproduction and NC DIS differ importantly by the absence or presence of a scattered electron in the ZEUS detector, respectively. The scattered electron in photoproduction typically remains undetected near the beam pipe, while in NC DIS, at increasingly large Q^2, the electron deflects increasingly into the detector. An offline event selection criteria for PhP (NC DIS) is defined according to this feature. The electron identification probability, as determined by a neural network algorithm using deposited energy in the CAL, was required to be less than 90% (greater than 90%). The scattered-electron energy in the CAL was larger than 10 (less than 15) GeV. The difference of the total observed energy and z-component of momentum, $E - p_Z$, was required to be less than 55 (between 47 and 69) GeV. In NC DIS, the virtuality, Q^2, as determined by the electron method [38] was greater than $5\,\mathrm{GeV}^2$. Events were required to contain a primary vertex near the centre of the detector: $|V_Z| < 30$ cm. At least 15% of the tracks reconstructed in the event were required to be associated with primary vertex to reject beam-gas background.

Reconstructed tracks were used in this analysis if their momentum transverse to the beam-axis and laboratory pseudorapidity were within $0.1 < p_{\mathrm{T}} < 5.0\,\mathrm{GeV}$ and $-1.5 < \eta < 2.0$, respectively. The track associated to the scattered electron candidate used to identify the NC DIS event was rejected in that part of the correlation analysis. Tracks corresponding closely to primary charged particles were selected in the analysis by requiring the distances of closest approach to the primary vertex in the transverse (DCA_{XY}) and longitudinal (DCA_{Z}) directions to be less than 2 cm.

High-multiplicity events were selected by requiring the number of charged primary particles in our kinematic acceptance, N_{ch}, to be at least 20. The contamination of PhP (NC DIS) events to the analysis of NC DIS (PhP) has been estimated to be on the order of 1% from studies of Monte Carlo data. A total of 5 (0.2) million PhP (NC DIS) events at high multiplicity passed the event-selection criteria. A more detailed description of event and track selection criteria can be found in an earlier ZEUS publication on this subject [15].

3 Monte Carlo generators

The modelling of photoproduction in *ep* scattering within the PYTHIA [26] Monte Carlo event generator has recently been developed [39]. PYTHIA was used for the extraction of efficiency corrections and the associated systematic uncertainties (version 6.220) and for the comparison of the photoproduction measurements to known physics mechanisms (version 8.303) in this analysis. For the DIS part of the analysis, the LEPTO 6.5 [40] and ARIADNE 4.12 [41] Monte Carlo event generators were used to extract efficiency corrections. The ZEUS detector was simulated using GEANT 3 [42]. Primary generated particles were defined as charged hadrons with a mean proper lifetime, $\tau > 1$ cm, which were produced directly or from the decay of a particle with $\tau < 1$ cm.

Both the direct and resolved components of photoproduction were included in the Monte Carlo samples in the proportion of about 1:100 for $N_{\rm ch} \geq 20$ as determined by PYTHIA. Partonic fluctuations arising from the quasi-real photon are parametrised with the CJKL [43] Parton Distribution Function (PDF). The quark and gluon content of the proton is parametrised with the NNPDF2.3 PDF [44]. Parton scattering between both PDFs in PYTHIA photoproduction is parametrised by the p_{T0} parameter, which regulates the IR divergences and adjusts the degree of MPI. The energy dependence of p_{T0} is parametrized as $p_{T0} = p_{T0}^{\rm ref}\,(W/7~{\rm TeV})^{0.215}$, where W is the centre-of-mass energy of the photon-proton system, which fluctuates event-by-event [26, 39]. Products of separate MPI subprocesses may further interact through the Colour Reconnection (CR) framework for which the range parameter is left at its default value or switched off (0). Colour reconnection is analogous to cross-MPI rescattering in Fig. 2.

The measurements shown in this article are compared to PYTHIA predictions with and without MPI. Three different degrees of MPI are chosen with $p_{T0}^{\rm ref}$ =2.5, 3.5, and 4.5, which are near a favored value of 3.0 previously found using charged particle distributions at HERA [39].

3.1 Efficiency corrections

The distributions and correlation functions measured in this analysis are affected by non-uniform particle tracking efficiency. Single-particle, pair, and quadruplet efficiencies are calculated as the ratio of reconstructed to generated particles, pairs, and quadruplets, respectively. Efficiencies are calculated differentially in ϕ, η, $p_{\rm T}$, and charge for single-particles; $\langle \eta_i - \langle \eta \rangle \rangle$, $\langle p_{T,i} - \langle p_{T,i} \rangle \rangle$, charge combination, and event multiplicity for pairs and quadruplets. Additionally, pair and quadruplet efficiencies are differentially calculated in the azimuthal quantities $\phi_1 - \phi_2$ and $\phi_1 + \phi_2 - \phi_3 - \phi_4$, respectively. Correction factors are given by the inverse of the efficiencies and are labelled $w_i^{(1)}$, $w_{ij}^{(2)}$, $w_{ijkl}^{(4)}$.

4 Analysis method

The two- and four-particle correlation functions are defined by

$$
\begin{aligned}
c_n\{2\} &= w_T \sum_e^{N_\mathrm{ev}} \left[\sum_{i\neq j}^{N_\mathrm{rec}} w_e\, w_{ij}^{(2)} \cos\left[n(\varphi_i - \varphi_j)\right]\right]_e \Bigg/ \sum_e^{N_\mathrm{ev}} \left[\sum_{i\neq j}^{N_\mathrm{rec}} w_e\, w_{ij}^{(2)}\right]_e ,\\
C_n\{4\} &= w_T \sum_e^{N_\mathrm{ev}} \left[\sum_{i\neq j\neq k\neq l}^{N_\mathrm{rec}} w_e\, w_{ijkl}^{(4)} \cos\left[n(\varphi_i + \varphi_j - \varphi_k - \varphi_l)\right]\right]_e \Bigg/ \sum_e^{N_\mathrm{ev}} \left[\sum_{i\neq j\neq k\neq l}^{N_\mathrm{rec}} w_e\, w_{ijkl}^{(4)}\right]_e ,
\end{aligned}
$$

where φ_i is the azimuthal angle of the particle i. The first and second harmonic ($n = 1-2$) are studied in this article. The first sum over e is performed for all events, N_ev, and the sums over i, j, k, l run over all selected charged particles in the event with multiplicity N_rec. Event weights are denoted by w_e and are used in the construction of four-particle cumulants. Trigger bias corrections are denoted by w_T and are unity for the NC DIS part of the analysis, which has an inclusive set of triggers. The photoproduction analysis is significantly affected by the available non-inclusive triggers. Simulations of the trigger in Monte Carlo data are used to calculate w_T, which is approximately 1.3 for the correlation functions. Two-particle azimuthal correlations are shown as a function of pseudorapidity difference $|\Delta\eta| = |\eta_1 - \eta_2|$, mean transverse momentum $\langle p_\mathrm{T}\rangle = (p_{\mathrm{T},1} + p_{\mathrm{T},2})/2$, and exchange photon virtuality Q^2.

Four-particle cumulant correlation functions are shown in this article and are defined by

$$
c_n\{4\}(p_\mathrm{T}\ \mathrm{poi}) = C_n\{4\}(p_\mathrm{T}\ \mathrm{poi}) - 2 \times c_n\{2\}(p_T\ \mathrm{poi}) \times c_n\{2\}.
$$

It is measured as a function of p_T poi (particle of interest), which refers to a specific p_T bin from which particle i in Eqs. 1 and 1 are chosen. Event weights are set to unity except in the construction of $c_n\{4\}$ in Eq. 1. To reduce the known bias to the cumulant construction caused by wide multiplicity bins [45], w_e is set to the number of pair or quadruplet combinations in Eq. 1 for $c_n\{2\}$ and $C_n\{4\}$, respectively.

Two-particle correlations are also reported in a two-dimensional form, which is defined as:

$$
C(\Delta\eta, \Delta\varphi) = \frac{S(\Delta\eta, \Delta\varphi)}{B(\Delta\eta, \Delta\varphi)},
$$

where $S(\Delta\eta, \Delta\varphi) = N_\mathrm{pairs}^\mathrm{same}(\Delta\eta, \Delta\varphi)$ and $B(\Delta\eta, \Delta\varphi) = N_\mathrm{pairs}^\mathrm{mixed}(\Delta\eta, \Delta\varphi)$ are the number of pairs for the signal and background distributions, respectively. These pair distributions were formed by taking the first particle from a given event and the other from either the same event or a different event (mixed) with similar values of N_rec and vertex Z position. The S distribution was corrected with $w_T\, w_{ij}^{(2)}$, while B was corrected with $w_i^{(1)} w_j^{(1)}$. Both distributions were symmetrised along $\Delta\eta$ and then individually normalised to unity before division.

The primary charged-particle multiplicity distribution, N_{ch}, is measured in photoproduction. Tracking efficiency corrections are performed using an unfolding procedure. The RooUnfold [46] Bayesian algorithm is used with the response matrix obtained from Monte Carlo data with the ZEUS detector simulation. Transverse momentum and η distributions (dN/dp_{T} and $dN/d\eta$) are also measured and corrected for tracking inefficiencies using the $w^{(1)}$ weight. Trigger bias correction factors are as large as 2 for dN/dN_{ch} and dN/dp_{T} for $N_{\mathrm{ch}} \lesssim 23$ and $p_{\mathrm{T}} \lesssim 0.5$ GeV, respectively.

High-multiplicity events are selected for the correlation functions, dN/dp_{T}, and $dN/d\eta$ distributions by calculating a weighted sum over the number of reconstructed tracks passing our selection criteria: $N_{\mathrm{ch}} = \sum_i^{N_{\mathrm{rec}}} w_i^{(1)}$.

5 Systematic uncertainties

Systematic uncertainties were estimated by comparing the distributions or correlations obtained with the default event- and track-selection criteria to those obtained with varied settings. The difference between the results obtained with the default and the varied settings was assigned as a signed systematic uncertainty. Positive and negative systematic uncertainties were separately summed in quadrature to obtain the total systematic uncertainty. A full description of the systematic studies performed for the NC DIS part of the analysis can be found in a related ZEUS analysis [15]. Variations of the track DCA, primary vertex position, low-p_{T} tracking efficiency, and different data-taking conditions were done identically for both NC DIS and PhP.

Additional systematic studies were performed for photoproduction (with typical values of the uncertainty given for $c_1\{2\}$ at low $\Delta\eta$). The available Monte Carlo photoproduction sample used to extract tracking-efficiency and trigger-bias corrections was biased by a jet preselection requirement. Another Monte Carlo data sample with much stricter jet preselections was utilized to estimate the corresponding bias to our corrections (symmetrised, $\sim +5\%$). The uncertainty from the trigger-bias correction was estimated by comparing the results obtained using three different sets of third-level triggers (symmetrised, $\sim -25\%$). After the application of tracking-efficiency corrections in Monte Carlo data, a residual difference remained between the reconstructed and generator-level distributions and correlations—Monte Carlo non-closure ($\sim -5\%$). The proportion of direct to resolved photoproduction events in the Monte Carlo data was varied from its default value to one where the direct component was removed ($\sim +1\%$). Offline cuts used to remove NC DIS events from the photoproduction sample were loosened from their default value to the one in parenthesis: $P_e < 0.9$ (0.98), $E_e < 15$ (30) GeV, $E - p_z < 55$ (65) ($\sim +10\%$).

6 Results

Figures 3 and 4 show $C(\Delta\eta, \Delta\varphi)$ in photoproduction and NC DIS for particles with $0.5 < p_{\mathrm{T}} < 5.0$ GeV, respectively. A dominant near-side ($\Delta\varphi \sim 0$) peak is seen at small $\Delta\eta$ and $\Delta\varphi$. On the away-side ($\Delta\varphi \sim \pi$), a broad ridge is observed. The peak and ridge structures are less pronounced in photoproduction than in NC DIS. There is no indication of a double-ridge, which was recently observed in high-multiplicity pp and p+Pb collisions [8–10].

The Q^2 dependence of two-particle correlations for the first and second harmonic are shown in Figs. 5 and 6, respectively. Photoproduction results are shown for the Q^2 interval from 0 to 1 GeV^2. Data in NC DIS starts at 5 GeV^2 where the scattered electron identification was reliable in HERA II. Results are presented for the full ranges of $|\Delta\eta|$ and p_{T}, and with a rapidity-separation condition, $|\Delta\eta| > 2$, for $p_{\mathrm{T}} > 0.1$ and $p_{\mathrm{T}} > 0.5$ GeV. Short-range correlations unrelated to collective behaviour are suppressed with the $|\Delta\eta|$ separation. Long-range ($|\Delta\eta| > 2$) correlations in heavy-ion collisions are known to increase with p_{T} up to a few GeV [7–13]. Above 5 GeV^2, the Q^2 dependence of long-range correlations is observed to be flat and the magnitude of $c_1\{2\}$ sharply decreases in photoproduction. Except for $c_1\{2\}$ with $p_{\mathrm{T}} > 0.5$ GeV, the magnitude of the correlations in photoproduction are significantly smaller than in NC DIS. The same observation can be made by comparing the size of the modulations in Fig. 3 to 4.

The charged particle multiplicity distribution in photoproduction corrected for tracking inefficiency and the trigger bias is shown in Fig. 7. The integral of the distribution in the range shown is normalised to unity. Expectations from PYTHIA are shown with varying degrees of MPI and colour reconnection. The mean number of MPI for each value of p_{T0}^{ref} is: 5.7 (p_{T0}^{ref} =2.5), 3.8 (p_{T0}^{ref} =3.0), 2.5 (p_{T0}^{ref} =3.5), and 2.1 (p_{T0}^{ref} =4.5). In the case where MPI was switched off (no MPI), the number of $2 \to 2$ parton scatterings is unity by definition. The effect of removing cross-MPI rescattering in Fig. 2 is equivalent to switching off colour reconnection between separate MPI (CR=0.0) and is shown for p_{T0}^{ref} =3.5 and increases the relative population of events at high multiplicity. The dN/dp_{T} and $dN/d\eta$ distributions of charged primary particles in photoproduction is shown in Figs. 8 and 9, respectively. The integral of the distributions in the ranges shown are normalised to unity. Both extremes of no MPI and high MPI are clearly disfavoured based on comparisons between data and PYTHIA.

Two-particle correlations as a function of $|\Delta\eta|$ for the first and second harmonic are shown in Figs. 10 and 11, respectively. At low $|\Delta\eta|$, the correlations are positive and decrease rapidly toward larger $|\Delta\eta|$. Long-range correlations at high $|\Delta\eta|$ are large and negative for $c_1\{2\}$, while being much smaller and positive for $c_2\{2\}$. In contrast, larger interaction regions display a different feature where the positive magnitude of $c_2\{2\}$ is much larger than the negative magnitude of $c_1\{2\}$ [47]. The no MPI expectation shows the most pronounced correlations, which appears diluted by the addition of more independent $2 \to 2$ parton scatterings (smaller p_{T0}^{ref}) between the photon and proton PDFs.

Two-particle correlations are shown as a function of $\langle p_{\mathrm{T}} \rangle$ for the first and second harmonic in Figs. 12 and 13, respectively. For both $c_1\{2\}$ and $c_2\{2\}$, the correlation strength grows with increasing $\langle p_{\mathrm{T}} \rangle$, which is universally observed in all collision systems [7–13].

Recent measurements of two-particle correlations in photo-nuclear ultra-peripheral Pb+Pb collisions at the LHC [14] have revealed significant long-range correlations as well. For a similar kinematic interval ($\langle N_{\mathrm{ch}} \rangle \sim 24$, $p_{\mathrm{T}} > 0.5$, $|\Delta\eta| > 2$) the extracted value of $v_{2,2}$ is approximately 0.001 and is consistent with the *ep* photoproduction values of $c_2\{2\} \sim v_{2,2}$ seen in Fig. 6. It should be noted that long-range correlations are expected in PYTHIA with or without colour reconnection as seen in Figs. 11 and 13 and are unrelated to hydrodynamic collective behaviour.

Four-particle cumulant correlations versus p_{T} poi are shown in Figs. 14 and 15 for the first and second harmonic, respectively. Two-particle correlations unrelated to collective behaviour are removed in the construction of the four-particle cumulant. Except for $c_1\{4\}$ at high p_{T} poi, the cumulant correlations are significantly positive, which indicate the presence of genuine four-particle correlations. This observation is in sharp contrast to measurements in non-fully-overlapping heavy-ion collisions where four-particle cumulants are observed to be negative [48], as expected from collective behaviour [24]. However, in small systems such as *ep* photoproduction, the eccentricity of the initial state as depicted in Fig. 2 fluctuates event-by-event and may lead to different expectations for the sign of the four-particle cumulant. Collisions from non-fully-overlapping heavy-ions are characterised by a persistent elliptical eccentricity which dominates the additional component induced by fluctuating parton distributions within the nucleus event-by-event.

While there is no consistent preference of the p_{T0}^{ref} parameter in PYTHIA in Figs.10–15, it is clear that the no MPI scenario is never favored. For the PYTHIA distributions and correlation function projections sensitive to MPI, the comparison to data provides a strong indication of MPI.

7 Summary and outlook

Measurements of charged-particle azimuthal correlations have been presented with the ZEUS detector at HERA in ep photoproduction and NC DIS at $\sqrt{s} = 318\,\mathrm{GeV}$ and $N_{\mathrm{ch}} \geq 20$, using an integrated luminosity of $366 \pm 7\,\mathrm{pb}^{-1}$. Charged particle multiplicity, transverse momentum, and pseudorapidity distributions have also been presented in photoproduction.

There is no clear indication of a double ridge in $C(\Delta\eta, \Delta\varphi)$ in neither photoproduction nor NC DIS at $Q^2 > 20\,\mathrm{GeV}^2$. The evolution of two-particle correlations with Q^2 clearly demonstrate that their strength in photoproduction is significantly smaller than in DIS. Long-range ($|\Delta\eta| > 2$) correlations observed here with $c_1\{2\}$ are much more negative than $c_2\{2\}$ is positive, which is not indicative of the kind of the collective behaviour associated with heavy-ion collisions. The results presented here complement a related ZEUS analysis of two-particle correlations in NC DIS [15].

The photoproduction measurements have been compared to PYTHIA expectations and the possibility of MPI in ep scattering has been investigated. The comparisons provide a strong indication of MPI. Similar conclusions have been made in a ZEUS analysis of three- and four-jet distributions [49]. For the PYTHIA predictions with MPI shown in this article, the mean number of distinct $2 \to 2$ initial parton scatterings per event in photoproduction ranged from 2 to 6. Other parameters in PYTHIA such as those pertaining to parton showering and hadronization are also expected to play an important role and should be investigated. The measurements also provide new constraints to the photon PDF, for which little data exists so far.

The measurements provide new insight into the features of azimuthal particle correlations in photon-initiated scattering. Future measurements with the Electron Ion Collider will be able to further test the possibility of MPI and a subsequent rescattering stage in even larger interaction regions.

Acknowledgements

We would like to thank Ilkka Helenius for many discussions concerning photoproduction in PYTHIA as well as Richard Lednicky for discussions of the spatial extent probed in *ep* scattering.

We appreciate the contributions to the construction, maintenance and operation of the ZEUS detector of many people who are not listed as authors. The HERA machine group and the DESY computing staff are especially acknowledged for their success in providing excellent operation of the collider and the data-analysis environment. We thank the DESY directorate for their strong support and encouragement.

References

[1] NA49 Collab., S.V. Afanasiev et al., Phys. Rev. **C 66**, 054902 (2002).

[2] BRAHMS Collab., I. Arsene et al., Nucl. Phys. **A 757**, 1 (2005).

[3] B.B. Back et al., Nucl. Phys. **A 757**, 28 (2005).

[4] STAR Collab., J. Adams et al., Nucl. Phys. **A 757**, 102 (2005).

[5] PHENIX Collab., K. Adcox et al., Nucl. Phys. **A 757**, 184 (2005).

[6] ALICE Collab., K. Aamodt et al., Phys. Rev. Lett. **105**, 252302 (2010).

[7] ALICE Collab., B. Abelev et al., Phys. Rev. **C 88**, 044910 (2013).

[8] CMS Collab., V. Khachatryan et al., JHEP **09**, 091 (2010).

[9] ALICE Collab., B. Abelev et al., Phys. Lett. **B 719**, 29 (2013).

[10] ATLAS Collab., G. Aad et al., Phys. Rev. Lett. **110**, 182302 (2013).

[11] ATLAS Collab., G. Aad et al., Phys. Rev. Lett. **116**, 172301 (2016).

[12] PHENIX Collab., A. Adare et al., Phys. Rev. Lett. **111**, 212301 (2013).

[13] PHENIX Collab., A. Adare et al., Phys. Rev. Lett. **115**, 142301 (2015).

[14] G. Aad and others.

[15] Abt, I. and others, JHEP **04**, 070 (2020).

[16] Miller, Michael L. and Reygers, Klaus and Sanders, Stephen J. and Steinberg, Peter, Ann. Rev. Nucl. Part. Sci. **57**, 205 (2007).

[17] E.V. Shuryak, Phys. Lett. **B 78**, 150 (1978). [Yad. Fiz. **28**, 796 (1978)].

[18] J.D. Bjorken, Phys. Rev. **D 27**, 140 (1983).

[19] U. Heinz and R. Snellings, Ann. Rev. Nucl. Part. Sci. **63**, 123 (2013).

[20] Piller, G. and Ratzka, W. and Weise, W., Z. Phys. A **352**, 427 (1995).

[21] Drescher, Hans-Joachim and Dumitru, Adrian and Hayashigaki, Arata and Nara, Yasushi, Phys. Rev. C **74**, 044905 (2006).

[22] D. Beavis et al., Phys. Rev. **C 44**, 1091 (1991).

[23] S. Voloshin and Y. Zhang, Z. Phys. **C 70**, 665 (1996).

[24] N. Borghini et al., Phys. Rev. **C 64**, 054901 (2001).

[25] A. Bilandzic et al., Phys. Rev. **C 89**, 064904 (2014).

[26] Sjöstrand, Torbjörn and Ask, Stefan and Christiansen, Jesper R. and Corke, Richard and Desai, Nishita and Ilten, Philip and Mrenna, Stephen and Prestel, Stefan and Rasmussen, Christine O. and Skands, Peter Z., Comput. Phys. Commun. **191**, 159 (2015).

[27] ZEUS Collab., U. Holm (ed.), *The ZEUS Detector*. Status Report, DESY (1993), doi:10.3204/PUBDB-2017-12635. `http://www-zeus.desy.de/bluebook/bluebook.html`.

[28] N. Harnew et al., Nucl. Instr. and Meth. **A 279**, 290 (1989).

[29] B. Foster et al., Nucl. Phys. Proc. Suppl. **B 32**, 181 (1993).

[30] B. Foster et al., Nucl. Instr. and Meth. **A 338**, 254 (1994).

[31] A. Polini et al., Nucl. Instr. and Meth. **A 581**, 656 (2007).

[32] M. Derrick et al., Nucl. Instr. and Meth. **A 309**, 77 (1991).

[33] A. Andresen et al., Nucl. Instr. and Meth. **A 309**, 101 (1991).

[34] A. Caldwell et al., Nucl. Instr. and Meth. **A 321**, 356 (1992).

[35] A. Bernstein et al., Nucl. Instr. and Meth. **A 336**, 23 (1993).

[36] W. H. Smith, K. Tokushuku and L. W. Wiggers, *Proc. Computing in High-Energy Physics (CHEP), Annecy, France, Sept. 1992*, C. Verkerk and W. Wojcik (eds.), p. 222. CERN, Geneva, Switzerland (1992). Also in preprint DESY 92-150B.

[37] P.D. Allfrey et al., Nucl. Instr. and Meth. **A 580**, 1257 (2007).

[38] S. Bentvelsen, J. Engelen and P. Kooijman, *Proc. Workshop on Physics at HERA*, W. Buchmüller and G. Ingelman (eds.), Vol. 1, p. 23. Hamburg, Germany, DESY (1992).

[39] Helenius, Ilkka, CERN Proc. **1**, 119 (2018).

[40] G. Ingelman, A. Edin and J. Rathsman, Comp. Phys. Comm. **101**, 108 (1997).

[41] L. Lönnblad, Comp. Phys. Comm. **71**, 15 (1992).

[42] R. Brun et al., GEANT3, Technical Report CERN-DD/EE/84-1, CERN, 1987.

[43] Cornet, F. and Jankowski, P. and Krawczyk, M. and Lorca, A., Phys. Rev. D **68**, 014010 (2003).

[44] Ball, Richard D. and others, Nucl. Phys. B **867**, 244 (2013).

[45] A. Bilandzic, R. Snellings and S. Voloshin, Phys. Rev. **C 83**, 044913 (2011).

[46] *Proceedings, PHYSTAT 2011 Workshop on Statistical Issues Related to Discovery Claims in Search Experiments and Unfolding, CERN,Geneva, Switzerland 17-20 January 2011*, in CERN Yellow Reports: Conference Proceedings, eds. Prosper, Harrison B. and Lyons, Louis. CERN, Geneva, 1 2011, doi:10.5170/CERN-2011-006.

[47] ALICE Collab., K. Aamodt et al., Phys. Lett. **B 708**, 249 (2012).

[48] Aaboud, Morad and others, Eur. Phys. J. C **77**, 428 (2017).

[49] Chekanov, S. and others, Nucl. Phys. B **792**, 1 (2008).

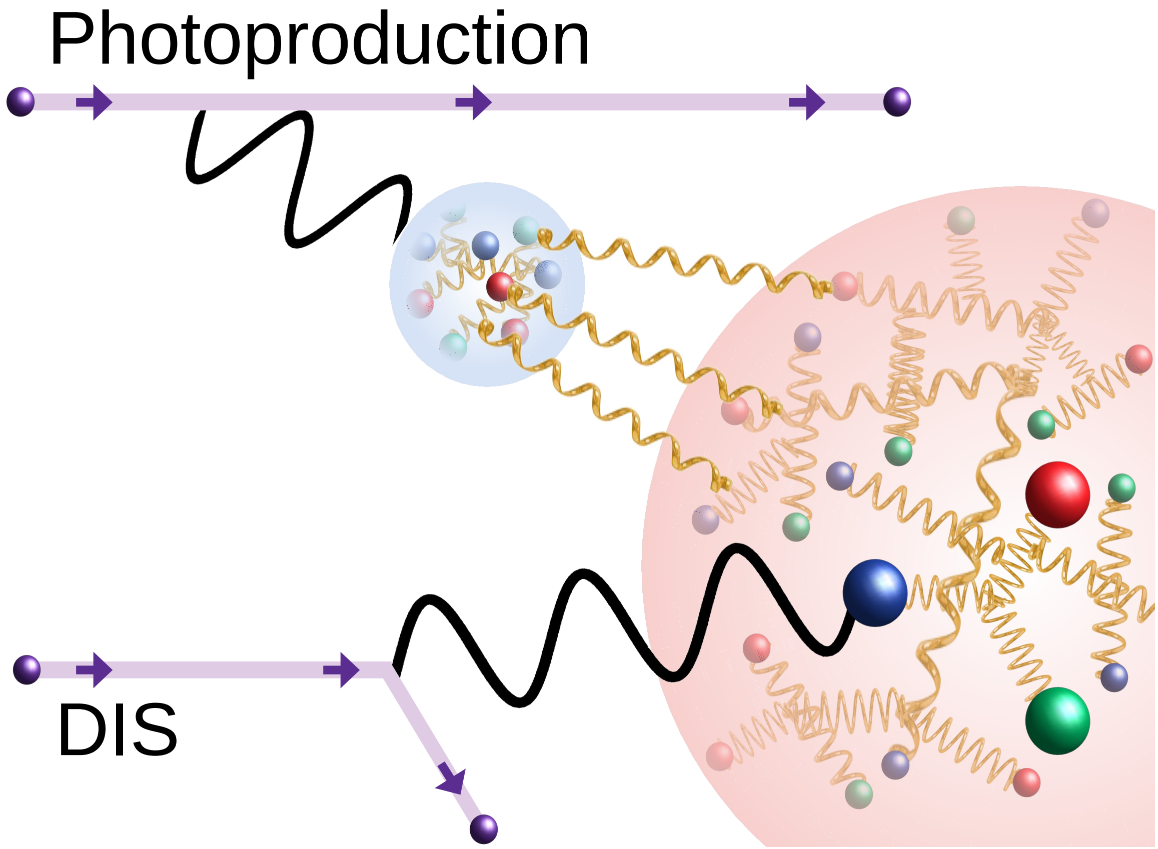

Figure 1: *Illustration of the initial scattering in two separate scenarios: resolved photoproduction and deep inelastic scattering at the top and bottom, respectively. The electron beam is represented by the lines with arrows. The proton and photon PDFs are shown as large and small pale circles, respectively. The exchanged photon is shown as a wavy line. Quarks are shown as spheres while gluons are shown as springs.*

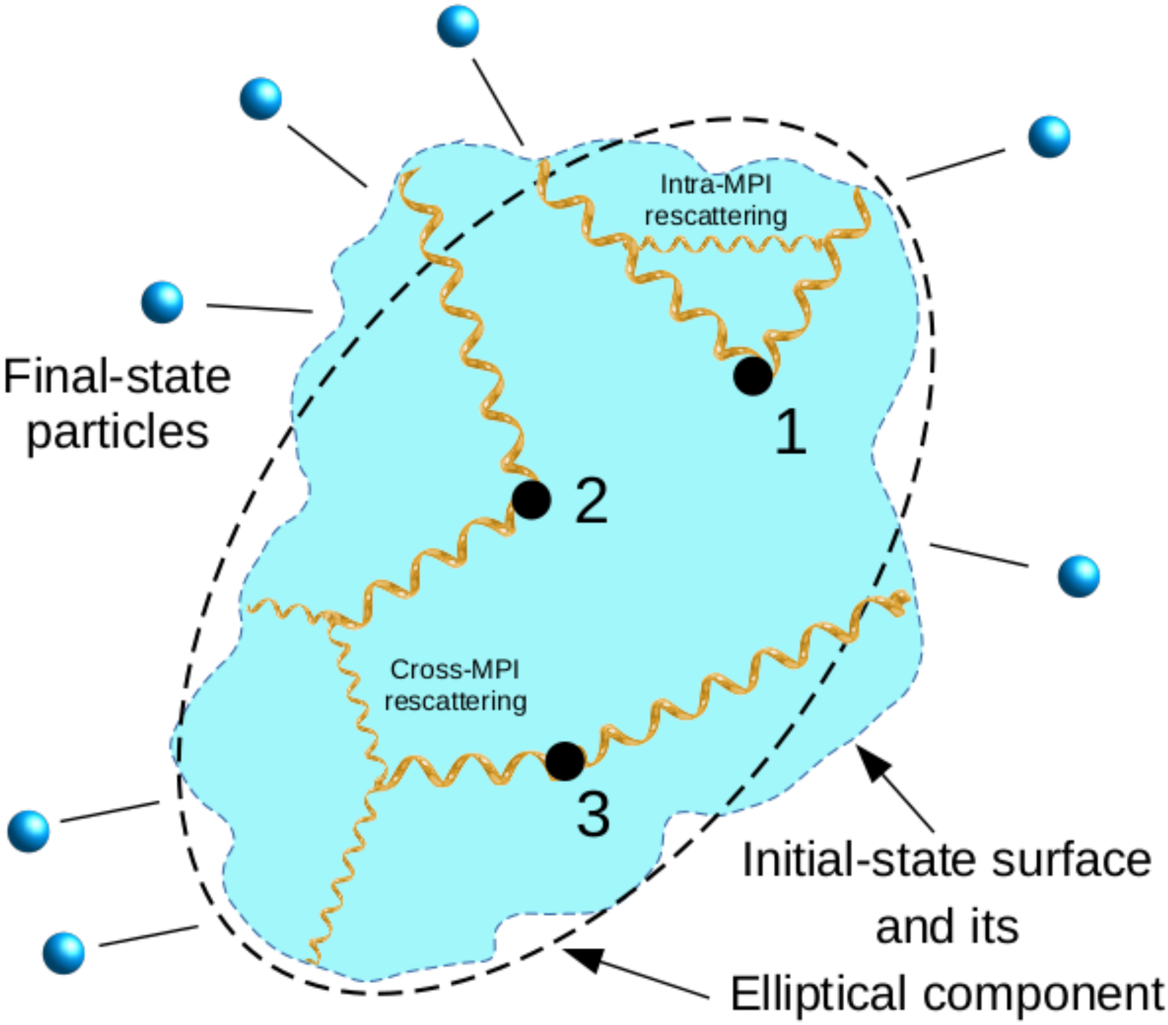

Figure 2: *Transverse view of the evolving collision zone after the initial scattering in resolved photoproduction. Three multiparton interaction (MPI) centers are shown with circles and act as sources of gluons. The possibilities of intra- and cross-MPI rescattering are illustrated near the top and bottom, respectively. Cross-MPI rescattering is akin to colour reconnection in PYTHIA. An initial state with a dominant elliptical eccentricity is shown.*

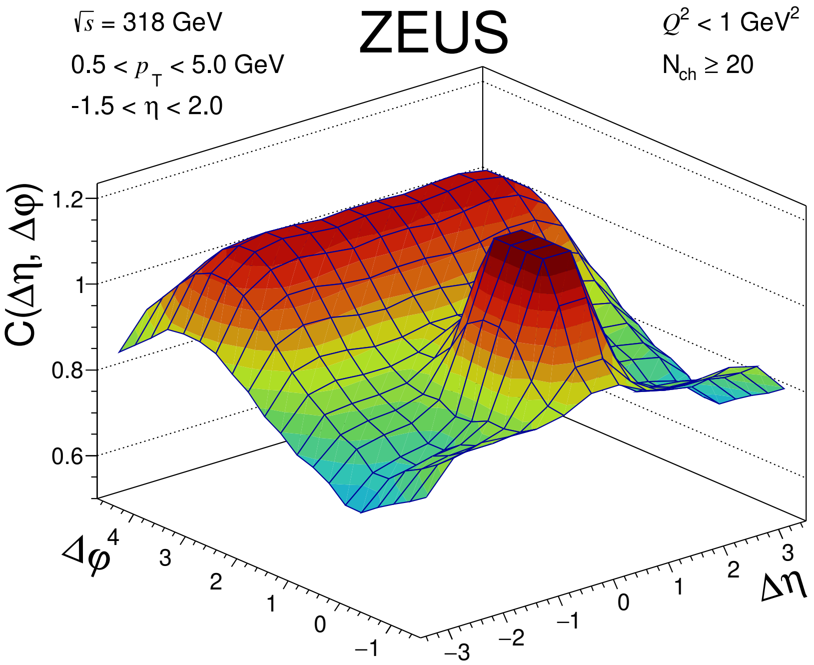

Figure 3: *Two-particle correlation $C(\Delta\eta, \Delta\varphi)$ in photoproduction. The peaks near the origin have been truncated for better visibility of the finer structures of the correlation. The plots were symmetrised along $\Delta\eta$. No statistical or systematic uncertainties are shown.*

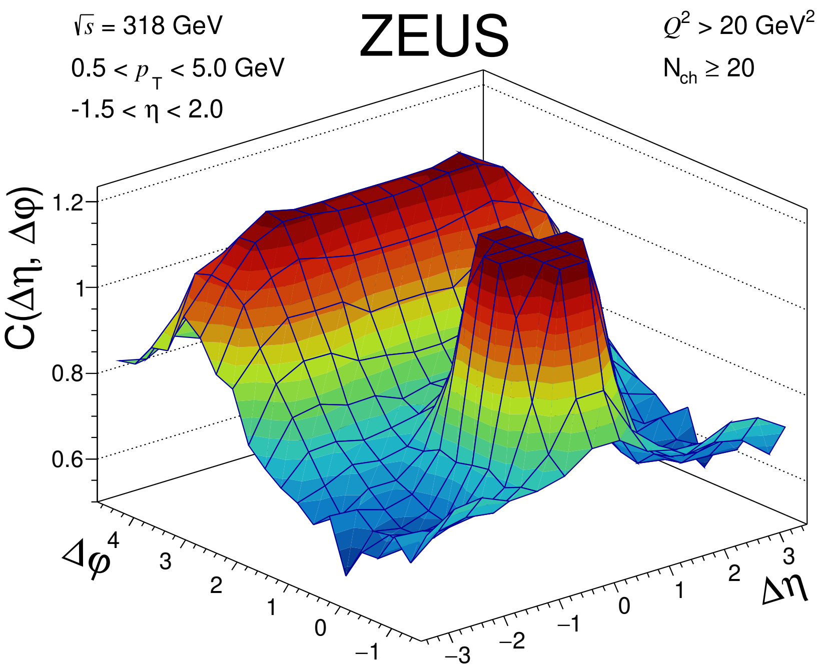

Figure 4: *$C(\Delta\eta, \Delta\varphi)$ in NC DIS with $Q^2 > 20$ GeV^2. The other details are as in figure 3.*

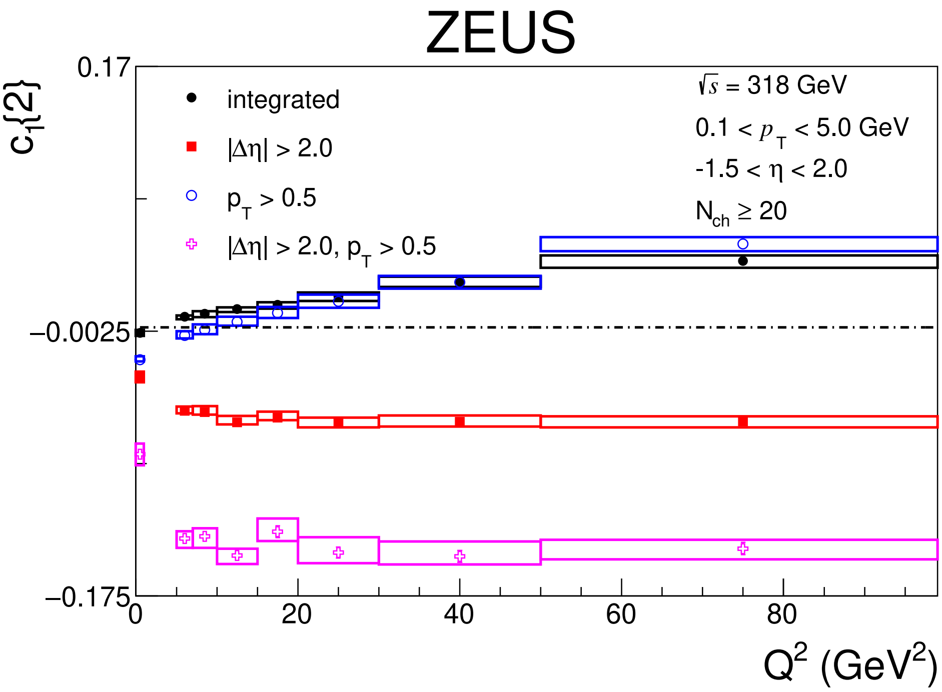

Figure 5: *Two-particle correlations $c_1\{2\}$ versus Q^2 with and without a rapidity separation, and for low- and high-p_{T} intervals. Photoproduction data is for $Q^2 < 1\,GeV^2$, while NC DIS is for $Q^2 > 5\,GeV^2$. Zero for $c_1\{2\}$ is indicated with a dot-dashed line. The statistical uncertainties are shown as vertical lines although they are typically smaller than the marker size. Systematic uncertainties are shown as boxes.*

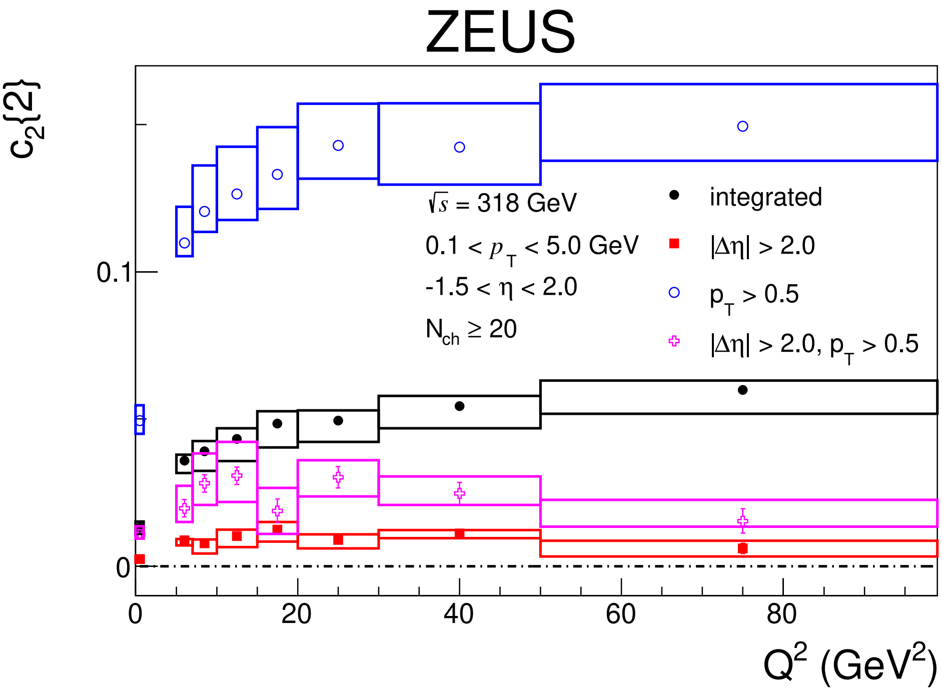

Figure 6: *Two-particle correlations $c_2\{2\}$ versus Q^2. The other details are as in figure 5.*

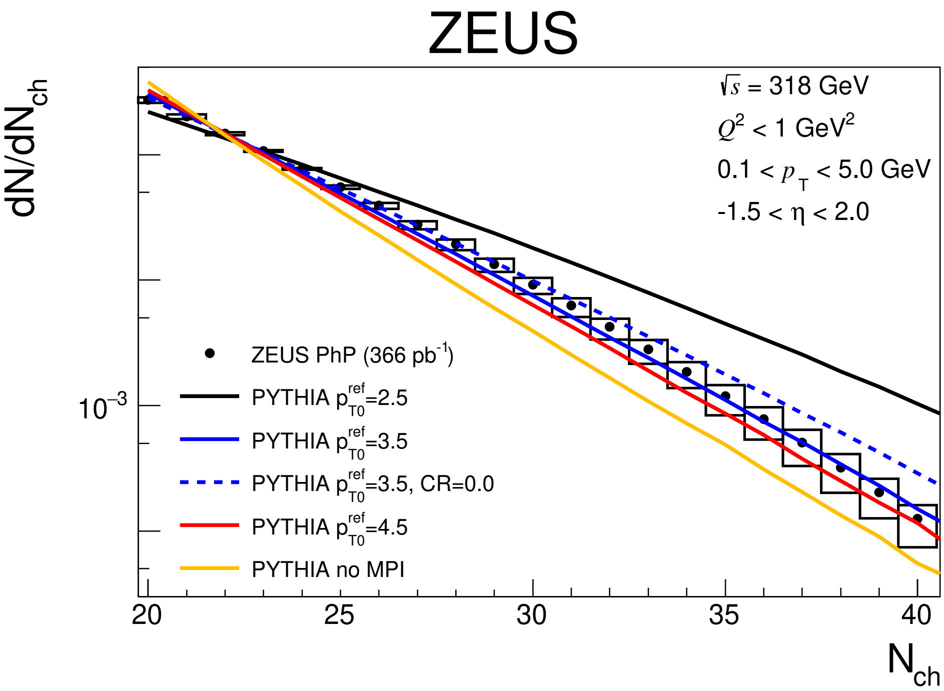

Figure 7: *Charged particle multiplicity distribution dN/dN_{ch} compared to PYTHIA expectations for different degrees of multiparton interactions (MPI), which is inversely related to $p_{T0}^{\rm ref}$. The mean number of MPI for each value of $p_{T0}^{\rm ref}$ is: 5.7 ($p_{T0}^{\rm ref}$ =2.5), 3.8 ($p_{T0}^{\rm ref}$ =3.0), 2.5 ($p_{T0}^{\rm ref}$ =3.5), and 2.1 ($p_{T0}^{\rm ref}$ =4.5). The dashed line corresponds to an expectation with colour reconnection switched off. The integral of the distributions in the range shown are normalised to unity. The statistical uncertainties are shown as vertical lines although they are typically smaller than the marker size. Systematic uncertainties are shown as boxes.*

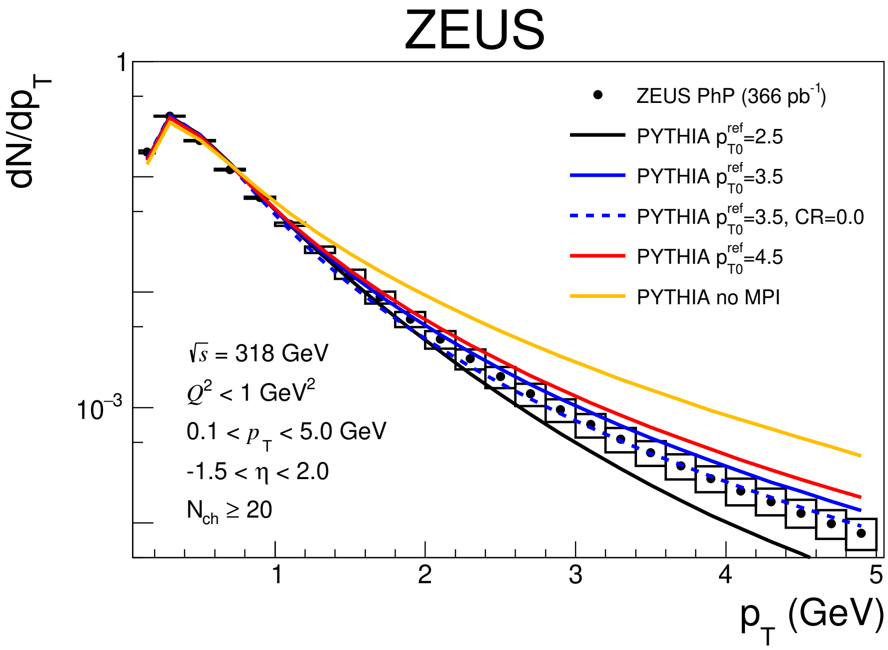

Figure 8: *Charged particle transverse momentum distribution dN/dp_{T} compared to PYTHIA expectations for different degrees of multiparton interactions (MPI). The other details are as in figure 7.*

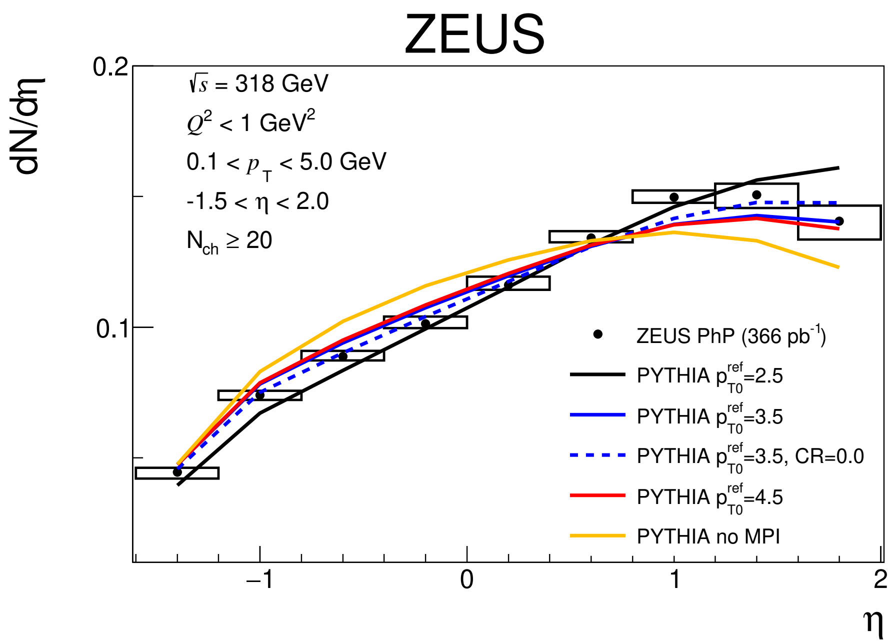

Figure 9: *Charged particle pseudorapidity distribution $dN/d\eta$ compared to PYTHIA expectations for different degrees of multiparton interactions (MPI). The other details are as in figure 7.*

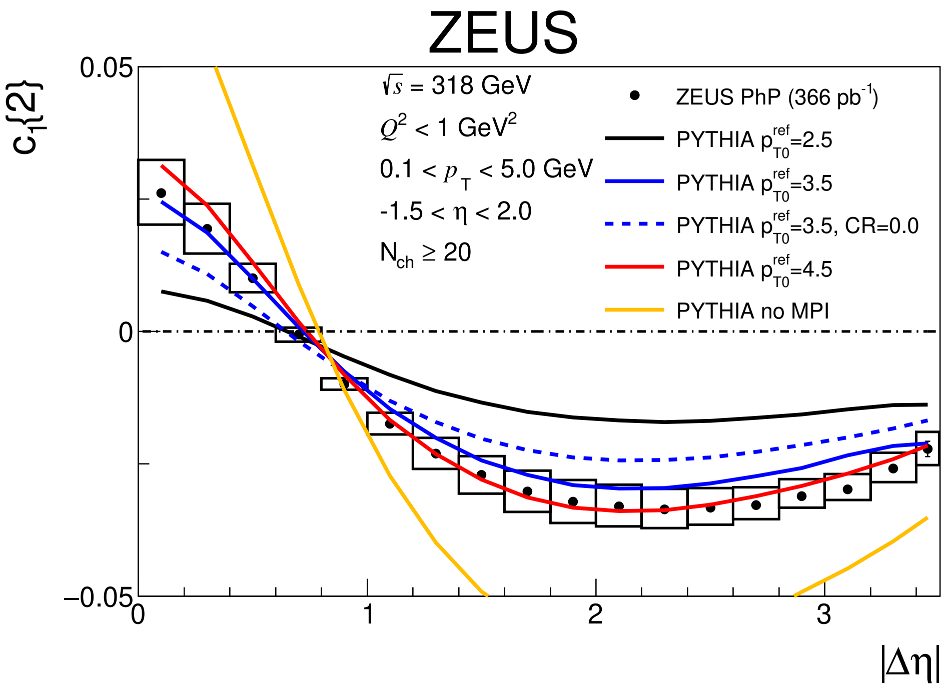

Figure 10: *Two-particle correlations $c_1\{2\}$ versus $|\Delta\eta|$ compared to PYTHIA expectations for different degrees of multiparton interactions (MPI). The other details (except for normalisation) are as in figure 7.*

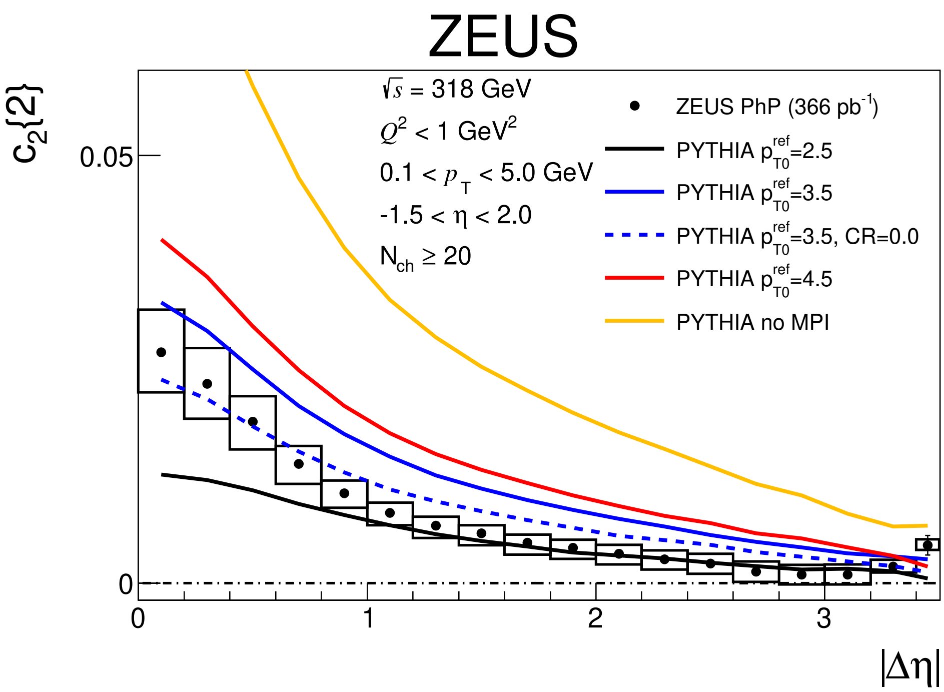

Figure 11: *Two-particle correlations $c_2\{2\}$ versus $|\Delta\eta|$ compared to PYTHIA expectations for different degrees of multiparton interactions (MPI). The other details (except for normalisation) are as in figure 7.*

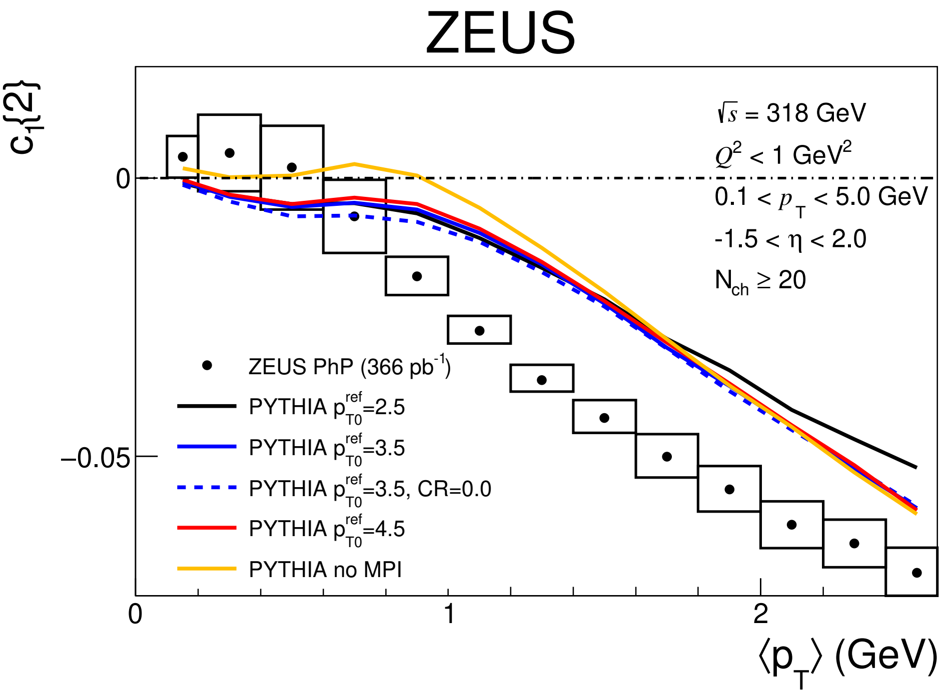

Figure 12: *Two-particle correlations $c_1\{2\}$ versus $\langle p_\mathrm{T}\rangle$ compared to PYTHIA expectations for different degrees of multiparton interactions (MPI). The other details (except for normalisation) are as in figure 7.*

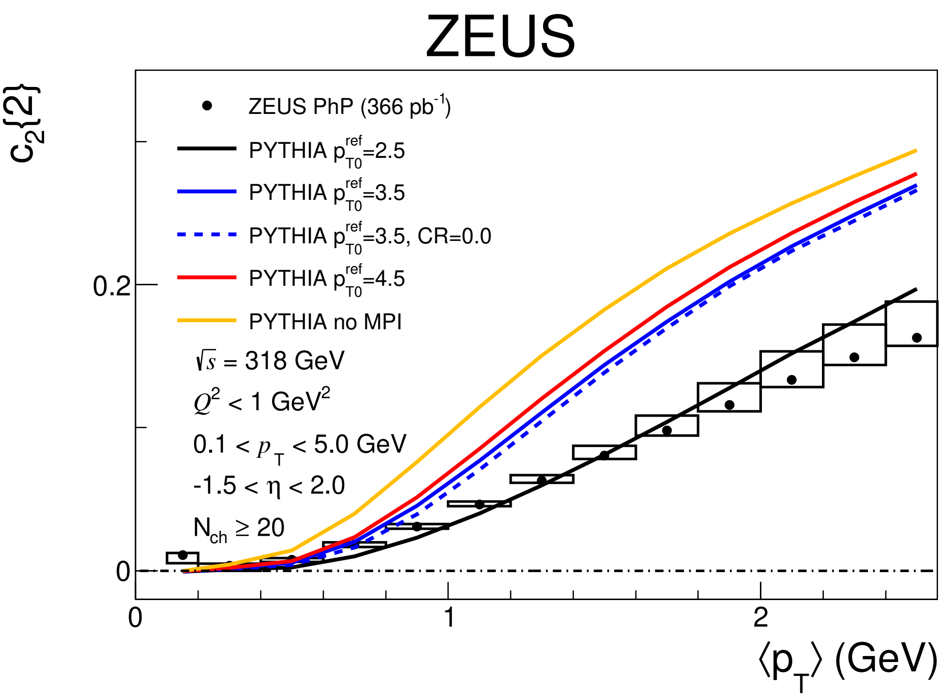

Figure 13: *Two-particle correlations $c_2\{2\}$ versus $\langle p_\mathrm{T}\rangle$ compared to PYTHIA expectations for different degrees of multiparton interactions (MPI). The other details (except for normalisation) are as in figure 7.*

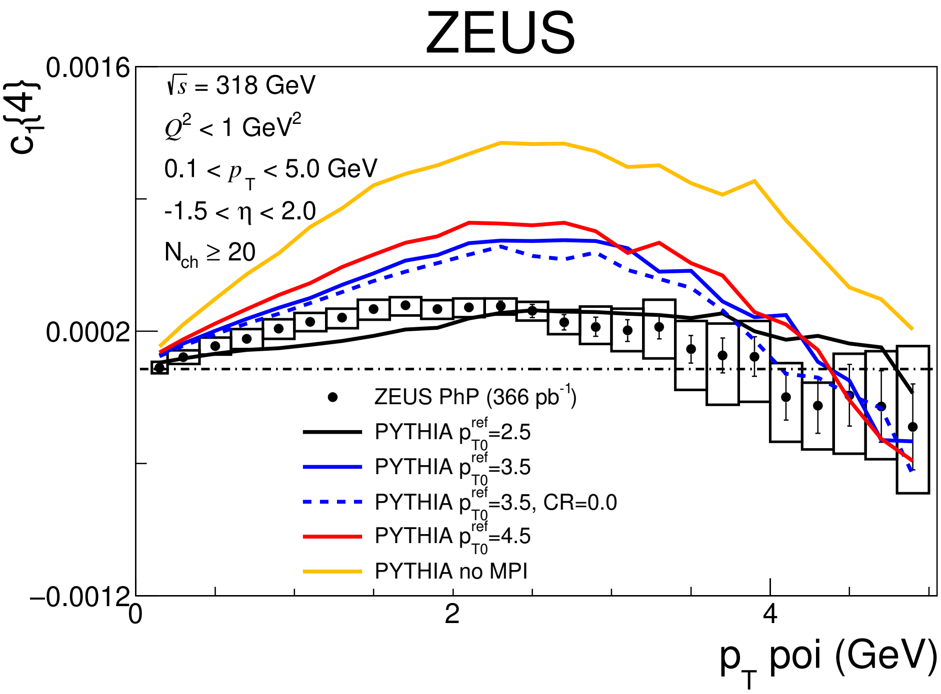

Figure 14: *Four-particle cumulant correlations* $c_1\{4\}$ *versus* p_T *poi compared to PYTHIA expectations for different degrees of multiparton interactions (MPI). The other details (except for normalisation) are as in figure 7.*

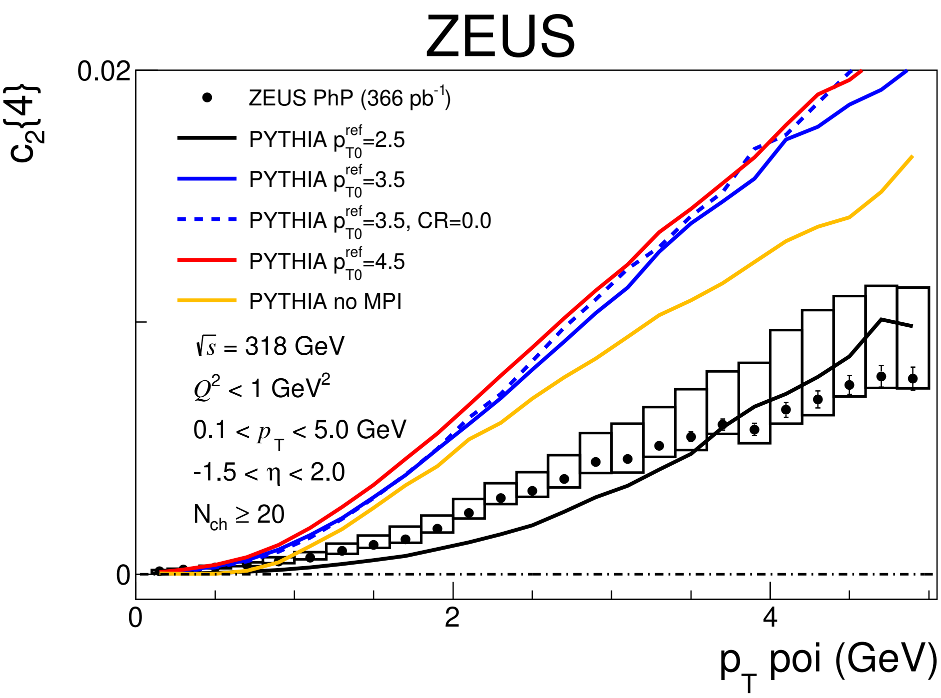

Figure 15: *Four-particle cumulant correlations* $c_2\{4\}$ p_T *poi compared to PYTHIA expectations for different degrees of multiparton interactions (MPI). The other details (except for normalisation) are as in figure 7.*